JOURNAL OF MATERIALS SCIENCE **36** (2001) 5271 – 5280

Zirconia-tungsten composites: synthesis and characterisation for different metal volume fractions

S. VIVES
CREST, UMR 6000-CNRS, Pole universitaire du pays de Montbéliard, 4 place Tharradin, BP 71427, 25211 Montbéliard, France
E-mail: serge.vives@pu.pm.univ-fcomte.fr

C. GUIZARD
IEM , UMR 5635-CNRS,UM II, CC 047, Place Eugène Bataillon, 34095 Montpellier cedex 5, France

C. OBERLIN
Electricité De France, Département Application de l'Electricité dans l'Industrie, Centre des Renardières, Route de Sens BP1, 77250 Moret sur Loing, France

L. COT
IEM , UMR 5635-CNRS,UM II, CC 047, Place Eugène Bataillon, 34095 Montpellier cedex 5, France

Zirconia-tungsten composites have been obtained by the densification of ceramic-metal powders. The influence of the sintering conditions and the metal volume fraction on the morphology, the porosity, the linear shrinkage, the microhardness and on the linear expansion coefficient has been evidenced. Using a general effective medium equation to fit the electrical resistivity of the composites (1400°C-3 h) a percolation threshold of 0.26 has been found. The distribution functions of relaxation times obtained from impedance spectroscopy measurements show that the higher is the thermal treatment the sharper are the peaks and the lower is the relaxation time τ_p. The intragrain zirconia ionic conductivity is improved for high tungsten volume fractions below the percolation threshold.

1. Introduction

Ceramic-metal materials obtained by powder mixture sintering are mainly studied for the improvement of the ceramic materials toughness [1, 2]. Indeed, introducing ductile metal particles in a ceramic matrix can increase the K_{IC} value of the resulting material. K_{IC} values in the range 5 MPa $\cdot$ m$^{1/2}$–8.5 MPa $\cdot$ m$^{1/2}$ have been reached for Ni/Al_2O_3 composites. These results are interesting knowing that $K_{IC}(Al_2O_3) = 3$ MPa $\cdot$ m$^{1/2}$.

The main parameter used to describe a composite material is the volume fraction for each phase. Most of the physical properties of such materials are volume fraction dependent like density, hardness, thermal expansion, thermal and electrical conductivity. The dc electrical conductivity is then very low, when the volume percent of the conductive particles (generally metal or carbon) is low, and increases very rapidly around a value called the percolation threshold. This threshold can be viewed as the point where a conductive network is built up by the contact of the conductive particles from one side to the other in the composite medium.

The aim of this work is to describe the synthesis of sintered zirconia-tungsten cermets obtained from composite powders and to characterise the evolution of the composite materials properties with the metal volume ratio. These materials could be interesting for the realisation of high temperature heating elements.

2. Experimental procedure

Composite zirconia-tungsten powders have been synthesised by ourselves using a "sol-gel/co-precipitation" route. This preparation is described elsewhere [3] but a scheme of the synthesis is given in Fig. 1. Different sintering conditions have been employed for the densification of the composite powders:

- cold pressing and sintering in H_2/Ar (10/90) atmosphere at 1400°C-3 h; 1400°C-10 h; 1500°C-8 h; 1850°C-30 min
- hot pressing (1450°C-300 kg/cm^2–10^{-4} mbar-30 min).

For each sample we have checked by X ray diffraction (Inel, Cu K_α radiation) that only the ZrO_2(c) and W phases were present in the composite. SEM observations were carried out with a JEOL microscope

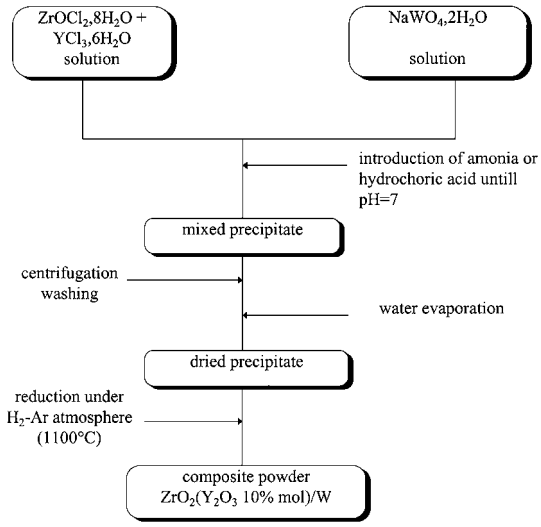

Figure 1 Scheme of the W/ZrO_2 powder synthesis.

to determine the morphology of the materials and the particle size of each phase.

The mercury porosimetry (Micromeritics) has been used to determine the pore size of the sintered materials. Before each measurement the samples were outgased at room temperature.

Linear shrinkage analysis and the determination of the linear thermal expansion coefficient have been performed with a Thermo Mechanical Analyse equipment (Setaram TMA) under flowing Ar (50 ml/min) for shrinkage measurements and under flowing He (50 ml/min) for thermal expansion measurements.

Indentation was performed using a Shimadzu microhardness tester with a Vickers diamond and an applied load lying between 100 g and 500 g.

A four probes method has been employed for the dc electrical conductivity measurements (AOIP OM 21 microohmmeter) both at room and high temperature. For ac measurements at room temperature a gain and phase equipment (Solartron 1253) was used, the frequency was in the range 10^{-3} Hz - 20 kHz. Measurements at high temperature were performed using a two terminal ac bridge (HP 4192M) between 5 Hz and 13 MHz. For both room and high temperature ac conductivity analysis Pt electrodes were sputtered on each side of the samples.

3. Results and discussion

3.1. Sintering and mechanical properties

The green density of composite materials obtained by mixing two powders influences the density of the resulting sintered materials for a given thermal treatment. The compactness of a random close packing of homodisperse spheres is 0.64. This compactness can be increased up to 0.74 by mixing two spherical powders with a radius ratio $r = r_{\text{matrix}}/r_{\text{inclusion}} < 0.1$ [4]. Results of green density measurements for different tungsten volume fractions are listed in Table I. The zirconia particle size is about 100 nm with a sharp distribution. For the tungsten crystals the size is in the range 0.1 μm–10 μm with a mean size about 6 μm–7 μm. Hence the condition $r_{ZrO2}/r_W < 0.1$ is fulfilled. We note a relative density of the zirconia powder below 0.64 meaning that this powder is not homogeneous and that agglomerates are surely present. For the composite powders the relative density is always above 0.64 implying a good homogeneity of the powders and a good dispersion of the inclusions.

TABLE I Relative green density for different metal volume fractions

W volume fraction (%)	Relative green density
0	0.58
17	0.68
32	0.67
51	0.65

After a sintering step at 1400°C-3 h we can observe a different morphology between a low (5 vol%) and a higher (30 vol%) metal content in the composite (Fig. 2). This different morphology arises from the first

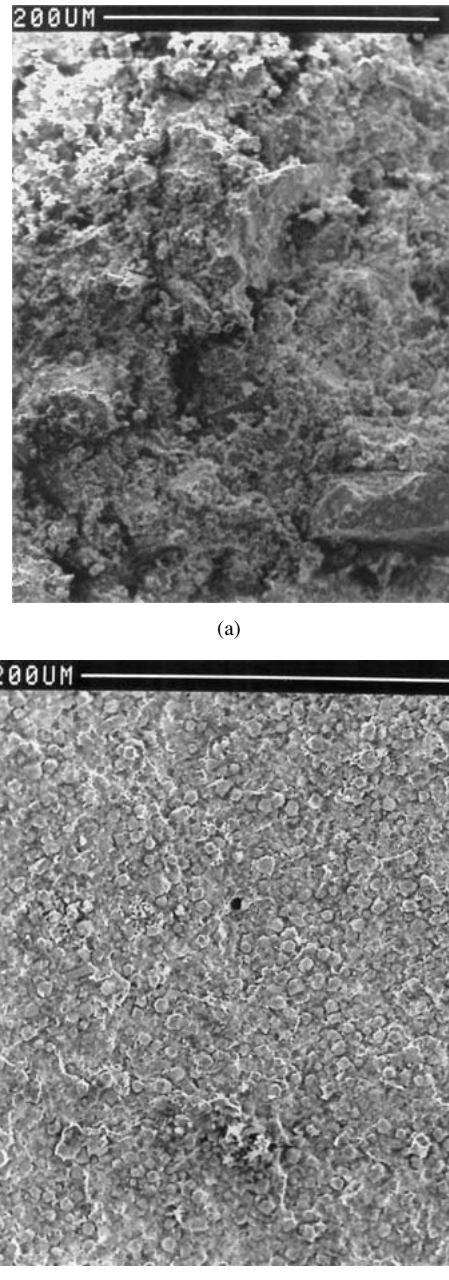

(a)

(b)

Figure 2 Morphology of the composite materials. a) W 5 vol%, b) W 30 vol%.

stage of the powder synthesis. It is know that zirconia obtained from a metal salt precipitation in an aqueous solution forms hard agglomerates. Indeed these agglomerates are the result of the surface hydroxyl groups condensation following [5, 6]:

$$-Zr_{surf}-OH + HO-Zr_{surf}- \rightarrow -Zr_{surf}-O-Zr_{surf}- + H_2O$$

Such hard agglomerates can not be broken by hand milling and consolidate during the thermal treatment, that what we see on Fig. 2a. Furthermore, we have shown [3] that the introduction of a tungsten salt in the solution leads to the zirconia surface recovery by charged tungsten species. This recovery creates repulsive interactions between grains thus improving the suspension stability and avoiding the formation of oxo bridges between the zirconia particles. This effect is always present after sintering as it is illustrated on Fig. 2b. Indeed during the reduction step the adsorbed tungsten oxides are reduced leading to a homogeneous distribution of tungsten crystals inside the zirconia matrix.

The density of the fully stabilised zirconia (Y_2O_3 10 mol%) is 5.929 g/cm^3 [7] and the tungsten one is 19.3 g/cm^3 [8]. According to the mixing rule the density of a W/ZrO_2 composite material is $d = 13.371x + 5.929$ (g/cm^3), where x is the tungsten vol%. Results of density measurements for different sintering conditions and different tungsten vol% are given on Table II. For a given thermal treatment the density increases with increasing tungsten vol% confirming that the composite powder homogeneity is improved. Although the increase of the temperature and dwell time leads to denser materials it is obvious that only the hot pressing technique is appropriate to reach relative densities of the cermet above 95%.

TABLE II Density of materials for various metal volume fractions and various sintering conditions

Tungsten vol%	Sintering conditions	Theoretical density	Experimental density	Relative density (%)
9,7	1400°C-3 h	7,22	5,02	69,5
19,7	1850°C-30 min	8,56	7,92	92,5
25	1400°C-3 h	9,25	6,72	72,6
25	1400°C-10 h	9,25	7,03	76
26	1450°C (hot pressed)	9,43	9,24	98
37	1400°C-3 h	10,87	8	73,6
37	1500°C-8 h	10,87	8,37	77
43,1	1400°C-3 h	11,69	9,6	82,1
43,1	1400°C-10 h	11,69	9,97	85,2

Results of porosimetry (Fig. 3) for samples sintered at 1400°C-3 h indicate that only one pore population is present whatever is the content of metal in the range 10 vol%–40 vol%. When the metal vol% is low (Fig. 3a) the peak is broad and asymmetric meaning a non uniformity of pore size. The peak becomes sharper and the pore diameter becomes smaller increasing the tungsten vol%, hence, for the same thermal treatment, the sintering is more efficient for a high tungsten content in the composite. The well defined and homogeneously distributed pores can be seen on Fig. 4 where a view of the surface sample (W 30 vol%) is presented. Although the density is higher for a thermal treatment at 1500°C

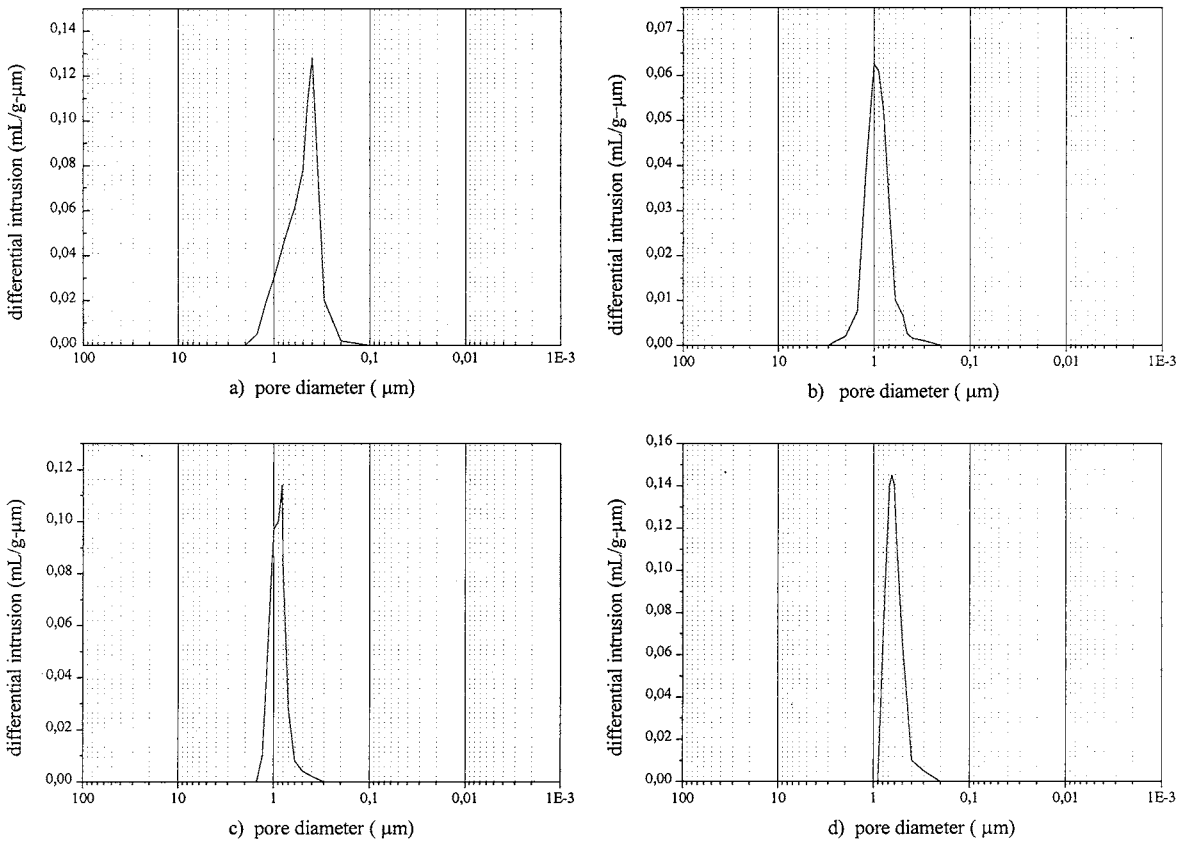

Figure 3 Results of the porosimetry measurements. a) W 9.7 vol%, b) W 25 vol%, c) W 35 vol%, d) W 42 vol%.

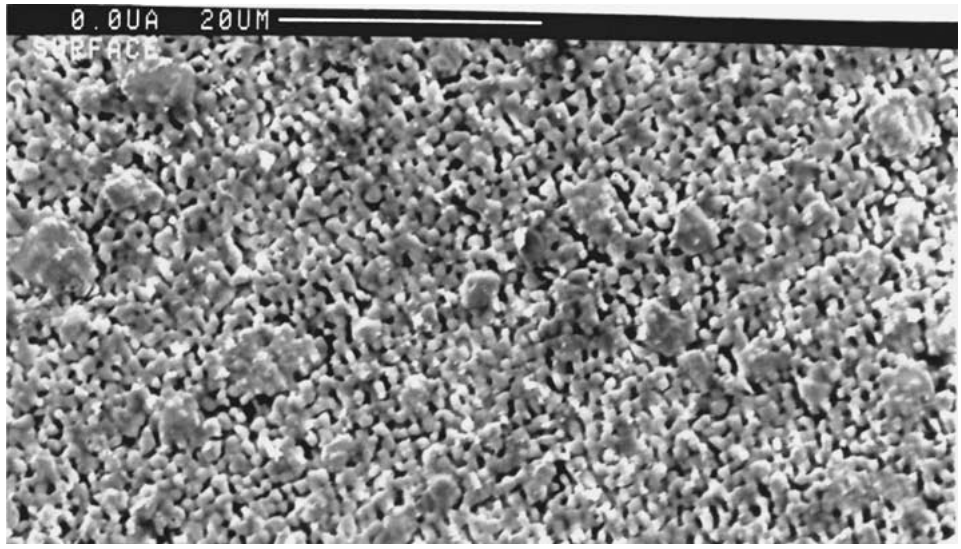

Figure 4 SEM surface view of a composite material (W 30 vol%-1400°C/3 h).

during 8 hours, we observe that the pore diameter is in the range 4 μm–5 μm. Obviously for hot pressing conditions no open porosity is detected in the material, but pores are observed inside the sample (Fig. 5).

For a given temperature and dwell duration the zirconia and tungsten particle size evolution is different. As we have mentioned before the zirconia grain size is about 100 nm at 1100°C. This size increases up to 1 μm–2.5 μm (1400°C-3 h), depending on the metal volume fraction, by a coarsening process which is greatly enhanced when the sintering is realised at 1500°C during 8 hours. Moreover it seems that the stabilisation of the zirconia cubic phase by the yttrium oxide implies a more important zirconia grain growth [9]. The tungsten crystal size does not vary very much in the range 1100°C–1400°C (3 h) and the distribution is always broad (0.1 μm–10 μm). The growth of tungsten crystals is evidenced for a thermal treatment at 1500°-8 h where the mean size is 15 μm, in these conditions the diffusion of the tungsten is improved. An illustration of the grain growth is given in Fig. 6. For a low sintering temperature (1200°C-3 h) grain and pore size is small and a high porosity is observed. For a high sintering temperature (1500°C-8 h) the porosity is lower but the pore and the grain sizes are larger.

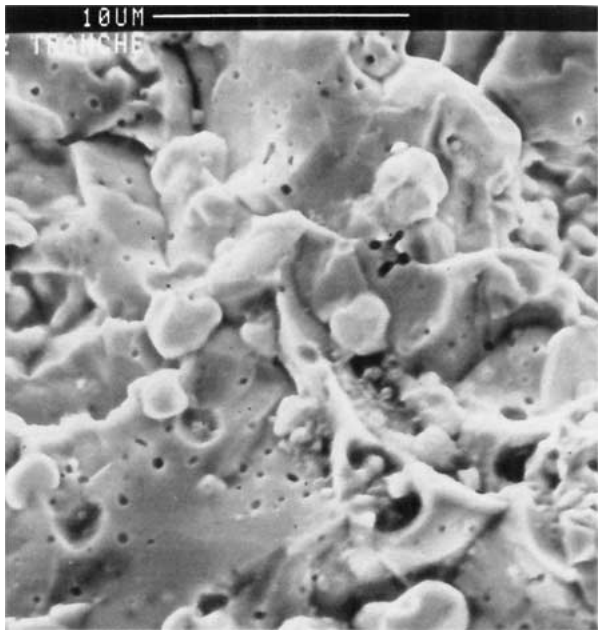

Figure 5 Closed porosity view of the hot pressed composite.

Linear shrinkage curves for different metal volume fractions are given on Fig. 7. We can note the effect of the tungsten addition on shrinkage. The metal acts as a hindrance or more precisely slows the shrinkage of the composite. This behaviour has already been reported for various composite materials. For ZnO matrix composites, the densification, for a given temperature, is always higher for the sole matrix than for the matrix reinforced with SiC particles [10] or zirconia particles [11]. This slowing densification effect could be due to stresses induced by the inclusions [12, 13] which can lead to cracks. For ours materials the shrinkage starts at 1100°C which is the powder synthesis temperature. It seems that only the matrix is involved in the linear shrinkage. At 1600°C the tungsten does not sinter even if a continuous metal network is formed inside the composite (43% tungsten volume fraction). Nevertheless, according to the density results, the relative density of the material increases with increasing the tungsten volume fraction for a given thermal treatment. For high tungsten volume fractions the densification is probably due to the zirconia grain coarsening. Indeed, the zirconia grain size, for a given thermal treatment (1400°C/3 h), evolves from 1 μm, for a 20% tungsten volume fraction, up to 2.5 μm for a 60% tungsten volume fraction. An expansion measurement has been performed for a 20% tungsten volume fraction composite up to 1850°C. For this temperature linear shrinkage reaches 12%. This value is inferior to the value obtained with the zirconia matrix treated at 1600°C but shows that a good densification of the composites needs a high temperature thermal treatment.

Results of Vickers microhardness measurements are presented on Fig. 8, all the samples were heat treated at 1400°C during 3 hours. The microhardness of the fully stabilised zirconia monocrystal is 16.1 GPa [14] and the

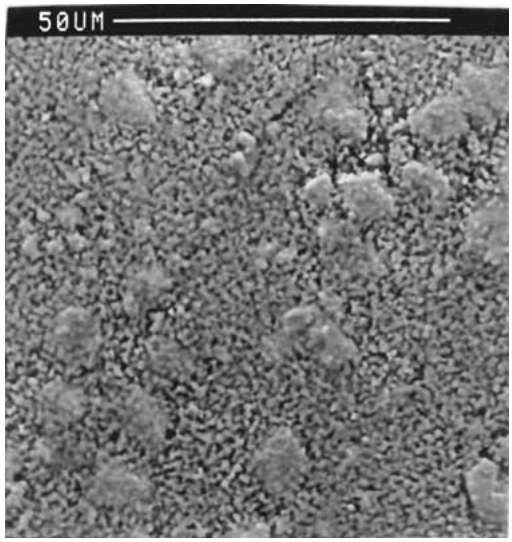

(a)

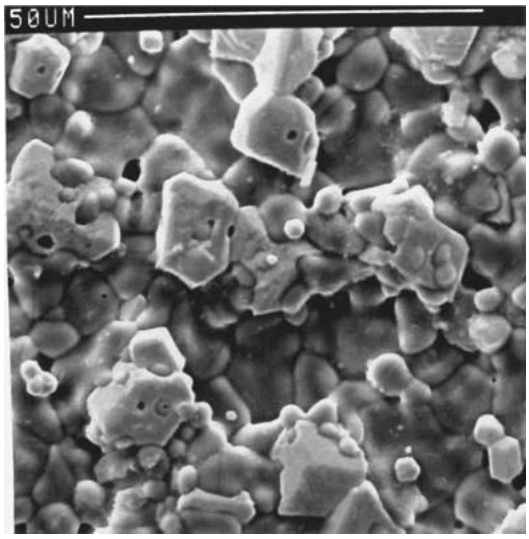

(b)

Figure 6 SEM surface views of a composite material. a) 1200°C-3 h, b) 1500°C-8h.

tungsten one is 2.25 GPa [15]. For low metal volume fractions materials the high microhardness is due to the zirconia which is a hard ceramic. The microhardness rapidly decreases between 10% and 40% metal volume fraction and does not evolve very much beyond this value. We can link this behaviour to the percolation effect. Beyond this threshold tungsten grains form a backbone which support a large part of the load. Similar results have been published. For a Ni-Al_2O_3 cermet Tuan [1] observes that the microhardness decreases from 16 GPa to 6 GPa when the Ni volume fraction increases from 0% to 25%, while Breval [2] obtains 9.6 GPa for a 50% Ni volume fraction. The discrepancy between these results could arise from different particle size or different material densities indicating the influence of the synthesis process on the microhardness. Results of the average expansion coefficient measurements between 20°C and 1000°C are summarised on Fig. 9. These results are compared with the mixing rule, the Turner model and the Kerner model. Turner [16] assumes that the material is isotropic on a macroscopic

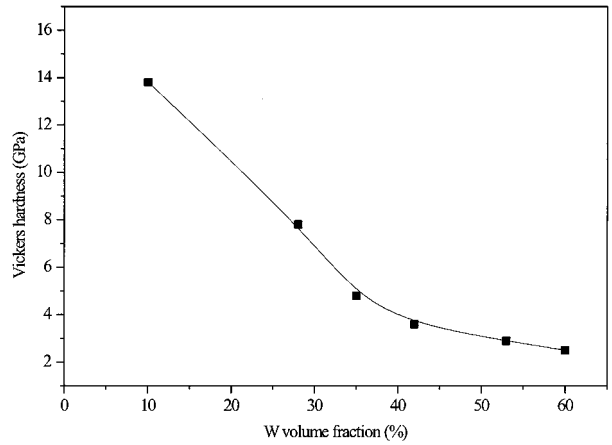

Figure 8 Vickers microhardness results.

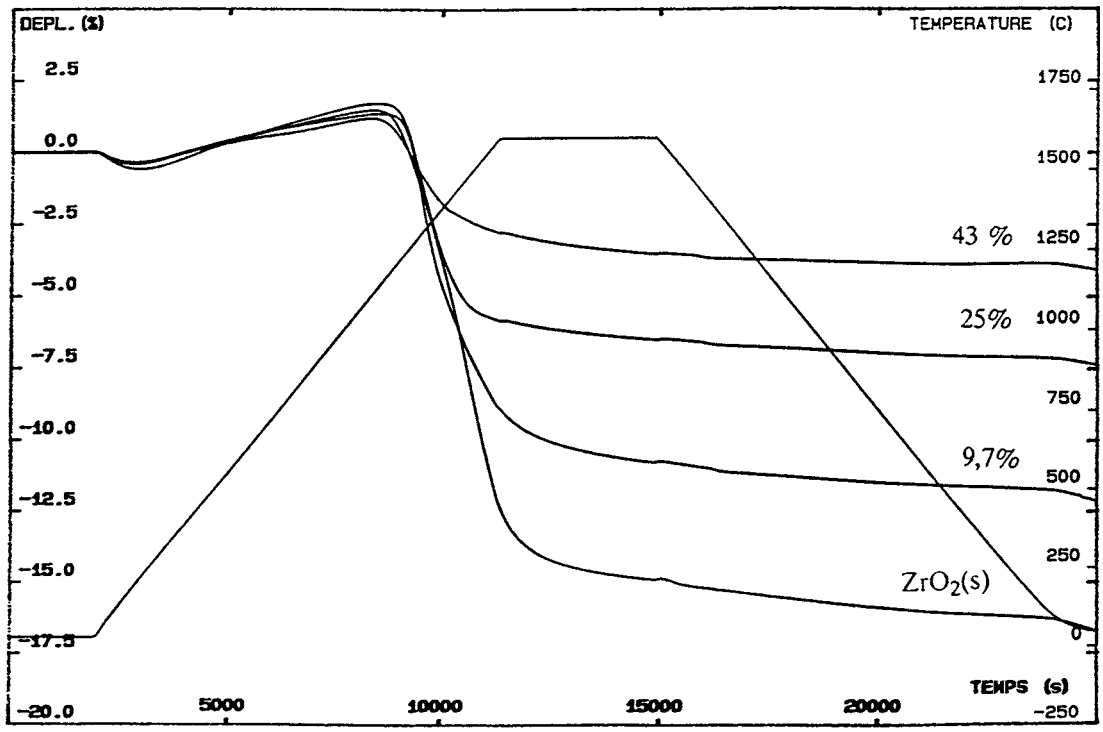

Figure 7 Linear shrinkage curves for various tungsten vol%.

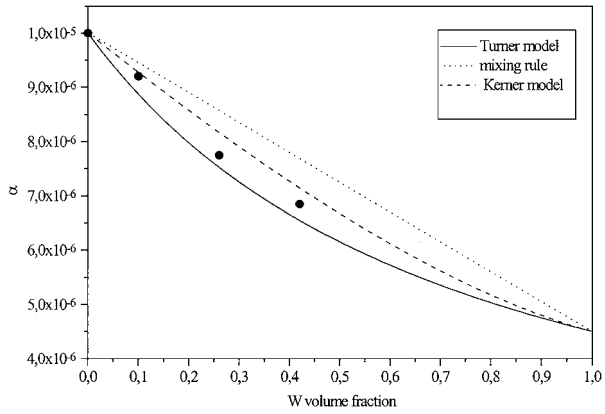

Figure 9 Comparison of thermal expansion coefficient measurements with the mixing rule, the Turner and the Kerner models.

scale, that a perfect adhesion exists between the two phases and that the strains of the two constituents are the same as the composite strains. Moreover, he admits that the internal stresses due to the increase of the temperature are not high enough to damage the material, he thus obtains the following expression:

$$\alpha = \frac{\alpha_m K_m c_m + \alpha_i K_i c_i}{K_m c_m + K_i c_i} \quad (1)$$

α: linear expansion coefficient of the composite, α_m, α_i: linear expansion coefficient of the matrix and the inclusions, K_m, K_i: bulk modulus of the matrix and the inclusions, c_m, c_i: volume fraction of the matrix and the inclusions.

Kerner [17] assumes that the grains are spherical and perfectly bounded to the matrix. He also takes into account the volume expansion and the shear stresses that exists between the matrix and the inclusions. He obtains the following expression:

$$\alpha = \alpha_m c_m + \alpha_i c_i - (\alpha_m - \alpha_i) c_m c_i \left[\frac{1}{K_m} - \frac{1}{K_i}\right] \times \left[\frac{c_m}{K_m} + \frac{c_i}{K_i} + \frac{3}{4G_m}\right]^{-1} \quad (2)$$

G_m: shear modulus of the matrix.
When $K_m = K_i$ these two expressions lead to the mixing rule:

$$\alpha = \alpha_m c_m + \alpha_i c_i \quad (3)$$

The zirconia and tungsten linear expansion coefficients, the bulk modulus and the shear modulus used for these models are listed in Table III.

For ours materials the linear expansion coefficients lie between the Turner and the Kerner models meaning that a good adhesion exists and that shear stresses are probably present between inclusions and matrix. Moreover no fracture have been observed for the composites whatever was the metal volume fraction.

TABLE III Values of α, K and G parameters

	W	ZrO_2 (10% Y_2O_3)
α	4.5 10^{-6}	10 10^{-6}
K	310 GPa	133 GPa
G	–	156 GPa

3.2. Electrical properties

At room temperature the electrical conductivity of the composite is due to the metallic phase. When the composite is a conductor its connectivity is 3-3 meaning that each phase is linked to itself in the 3 dimensions [18]. At the percolation threshold the connectivity of the material evolves from 0-3 to 3-3. This transition is difficult to visualise using electronic microscopy techniques. On Fig. 10 are presented backscattered electrons views of the composites, sintered at 1400°C during 3 hours, for different tungsten volume fractions. For a low metal content (8 vol%), the number of tungsten crystals is low and the distribution is non homogeneous (Fig. 10a). Zirconia agglomerates are present in the starting powder and during the reduction step tungsten species lead to large tungsten crystals between theses agglomerates. For a 25% metal volume fraction (Fig. 10b), the distribution of tungsten crystals inside the oxide matrix is more homogeneous. For this metal content the percolation threshold is not reached. Above the percolation threshold (45 vol%), the number of tungsten crystals is high and the distribution is uniform at the scale under consideration (Fig. 10c) even if it is difficult to evidenced a percolating way. We thus see that the sol-gel process leads, for metal volume fractions high enough (>20 vol%), to composite materials where the metal is homogeneously distributed without mixing and milling steps.

Results of the electrical resistivity measurements, for composites sintered at 1400°-3 h, are presented on Fig. 11, experimental data have been fitted using the general effective medium equation (G.E.M) [18]:

$$\frac{(1-f)\left(\rho_m^{1/t} - \rho_h^{1/t}\right)}{\rho_m^{1/t} + A\rho_h^{1/t}} + \frac{f\left(\rho_m^{1/t} - \rho_I^{1/t}\right)}{\rho_m^{1/t} + A\rho_I^{1/t}} = 0 \quad (4)$$

ρ_m: composite resistivity, ρ_h: non conductive phase resistivity, ρ_l: conductive phase resistivity, $A = (1 - f_c)/f_c$: f_c being the percolation threshold f: conductive phase volume fraction (metal volume/sample volume), t: parameter.

The tungsten electrical resistivity is 5.65 $\mu\Omega \cdot$cm [19] and the zirconia one is $8.2 \times 10^{12} \mu\Omega \cdot$cm [20]. For low metal volume fractions (<25 vol%) no percolation cluster exists, the resistivity is high and does not evolve very much. Around the percolation threshold clusters are created at random. The increase of the metal volume fraction leads to the occurrence of more percolation clusters with a higher average section and a lower average turtuosity thus decreasing the resistivity of the composite. Using this model the percolation threshold is 0.26 and the t parameter is 3.5. The percolation threshold of a composite material can vary according to the synthesis process, the inclusions shape and size or the percolation model used. Chen and Johnson [21] find a percolation threshold as low as

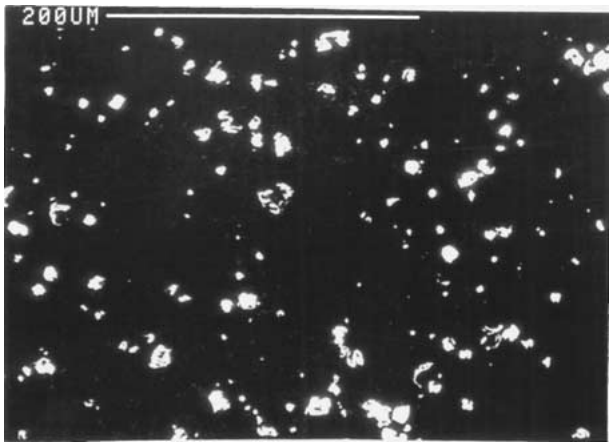

(a)

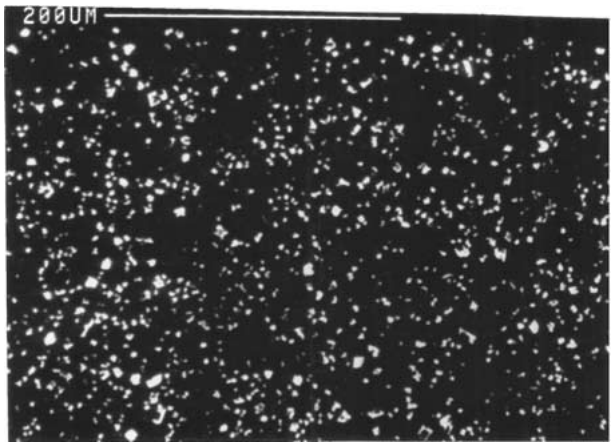

(b)

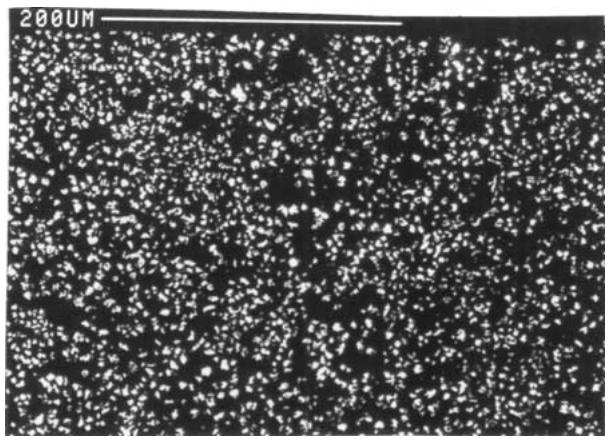

(c)

Figure 10 Backscattered electrons views of composite materials for various tungsten vol%. a) W 8 vol%, b) W 25 vol%, c) W 45 vol%.

0.08 for a Ni/polypropylene composite with filamentary shape inclusions and 0.27 for nodular shape inclusions, Abeles *et al*. find 0.47 for W/Al_2O_3 thin films [22]. For a hot pressed pellet with 20% tungsten volume fraction the resistivity was $3 \times 10^{-3}\ \Omega \cdot cm$ showing the influence of the density on the percolation threshold. The t parameter is related to the fractal dimension of the percolation clusters. This parameter generally lies between 1.65 and 2 for a composite medium with spherical inclusions distributed at random. Recently t parameter in the range 3–6 have been found for metal-insulator composite materials [23–25] araising from the microstructure of the compacts and the presence of porosity.

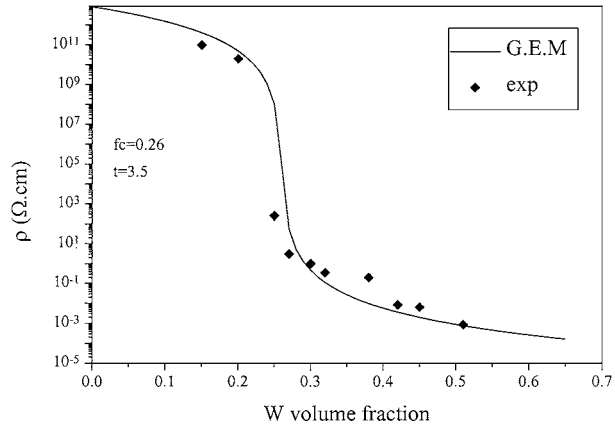

Figure 11 Fit of the electrical resistivity of the composites by a general effective medium equation.

The evolution of the dc electrical resistivity, of a 45% tungsten volume fraction composite, with the temperature is compared with the tungsten electrical resistivity [19] on Fig. 12. For both materials the resistivity increases with temperature which evidenced the metallic nature of the conductivity. We can note a different slope for the composite and the pure tungsten, the lower slope of the composite can be related to the ionic conductivity of the stabilised zirconia which is surely enhanced by the thermal treatment under reducing atmosphere. Some oxygen vacancies have been created by such a thermal treatment thus improving the ionic conductivity of the zirconia for the range of temperature under investigation. According to the linear fits, the temperature coefficients of resistivity (TCR) in the range 20°C–400°C are $4.89 \times 10^{-3}/°C$ and $5.21 \times 10^{-3}/°C$ for the tungsten and the composite respectively.

Samples with tungsten volume fractions (14% and 20%) below the percolation threshold have been characterised using the impedance spectroscopy at room temperature. The interest of this characterisation is to obtain qualitative informations about the ceramic-metal interface from the distribution function of relaxation times. Indeed dielectric materials could be modelled by an equivalent electrical circuit shown on Fig. 13. The complex impedance of such a circuit is given by the relation:

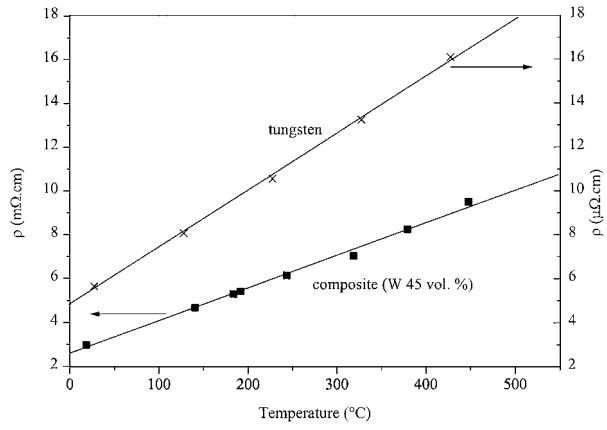

Figure 12 Comparison of the temperature dc electrical resistivity dependence for a composite material and pure tungsten.

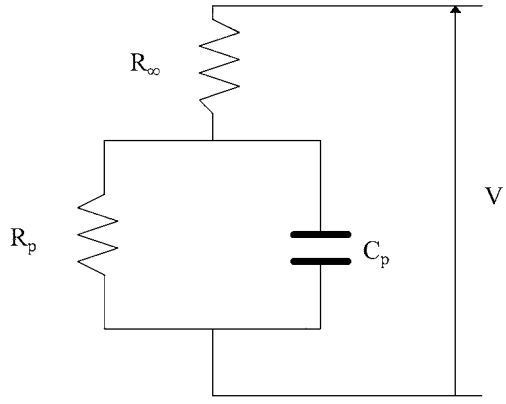

Figure 13 Scheme of the equivalent electrical circuit.

$$Z(\omega) = R_\infty + \frac{R_{0\infty}}{1 + j\omega\tau_p} \tag{5}$$

R_∞ is the resistance for a infinite frequency, R_0 is the resistance for a 0 frequency, $R_{0\infty} = R_0 - R_\infty$, $j^2 = -1$ and $\tau_p = R_p C_p$. The above equation can be written in the following form:

$$[R(\omega) - (R_p + R_\infty)/2]^2 + [X(\omega)]^2 = 1/4(R_p - R_\infty)^2 \tag{6}$$

which is a semicircle equation centred on the $R(\omega)$ axis. $R(\omega)$ and $X(\omega)$ are the real and the imaginary part of the impedance $Z(\omega)$. The relaxation time τ_p is defined as $\tau_p = 1/\omega$ with ω taken at the top of the semicircle. This impedance diagram describes the ideal Debye case. For a real case the centre of the semi circle is situated below the real axe forming with it an angle θ. The Cole-Cole [26] model is then necessary to study the behaviour of the material under an alternative voltage. An example of such a diagram, often called Nyquist plot is presented on Fig. 14. The complex impedance becomes:

$$Z(\omega) = R_\infty + \frac{R_{0\infty}}{(1 + j\omega\tau_p)^{1-\beta}} \tag{7}$$

$\beta = 2\theta/\pi$ and can be seen as a heterogeneity parameter. Once this parameter is known it is possible to have

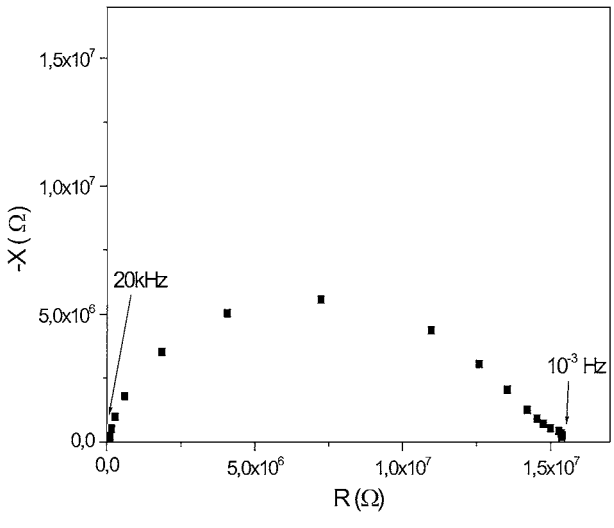

Figure 14 Nyquist plot of a composite material (20 vol%).

the distribution function of relaxation times using the following expression:

$$F(t) = \frac{1}{2\pi} \frac{\sin(\beta\pi)}{\cosh[(1-\beta)s] - \cos(\beta\pi)} \tag{8}$$

with $s = \ln(\tau/\tau_p)$.
The study of the distribution of relaxation times for percolating systems have recently been reported [27].

For a homogeneous material $F(t)$ will be a Dirac peak centred on $\tau = \tau_p$. The peak will be broader for a large distribution of relaxation times meaning a non homogeneity of relaxing species which, in our case, are space charges blocked at the ceramic-ceramic or ceramic-metal interfaces. Figs 15a and 15b present the influence of the tungsten volume fraction, for two different thermal treatments, on the distribution function of relaxation times. The relaxation time τ_p is longer when the metal volume fraction is increased in the composite. This could be due to a higher number of tungsten crystals and thus a higher number of ceramic-metal interfaces which leads to a longer return to equilibrium time of the relaxing species. Broader peaks are also observed when the tungsten content is increased, this could be link to the higher number and a non homogeneity (shape and size) of the ceramic-metal interfaces. The effect of the thermal treatment on $F(t)$ is revealed on Figs. 15c and d. We notice that the peak becomes sharper for the high temperature thermal treatment (1500°C-3 h), this is clearly seen for the 14% tungsten volume fraction composite but it is also true for the 20 vol% composition sample. Moreover the peak is shifted towards lower times. It seems that the high temperature sintering homogenises the material improving the tungsten crystals size distribution which becomes sharper and accentuating the geometrical ceramic-metal interfaces similarity. The peak position shift could be linked to an improvement of the ceramic-metal interface quality (tight contact) and to the material densification. As it is also noted by Lu *et al.* [28], for Ni-Al_2O_3 cermets, we believe that space charges polarization plays a dominant role in the dielectric behaviour of composites.

The ionic conductivity of the stabilised zirconia arises from the addition of yttrium oxide which creates some oxygen vacancies in the fluorite structure according to the following reaction:

$$Y_2O_3 \rightarrow 2Y'_{Zr} + V_{\ddot{o}} + 3O^x_o$$

Y'_{Zr} is the substitution of Y for Zr in the fluorite lattice, O^x_o is the lattice oxygen and $V_{\ddot{o}}$ the oxygen vacancy. The ionic conductivity is due to the movement of oxygen from site to site (vacancy) under the electric field and temperature. Arrhenius plots of the intragrain ionic conductivity of the zirconia for two composite materials (9 vol%, 14 vol%) are presented on Fig. 16. As it can be noted the three lines are parallels indicating that the tungsten have no influence on the activation energy of the stabilised zirconia intragrain ionic conductivity. This activation energy (1.13 eV) is equal to the energy found by Schouler *et al.* [29]. Nevertheless, the presence of the metal phase improves the ionic conductivity

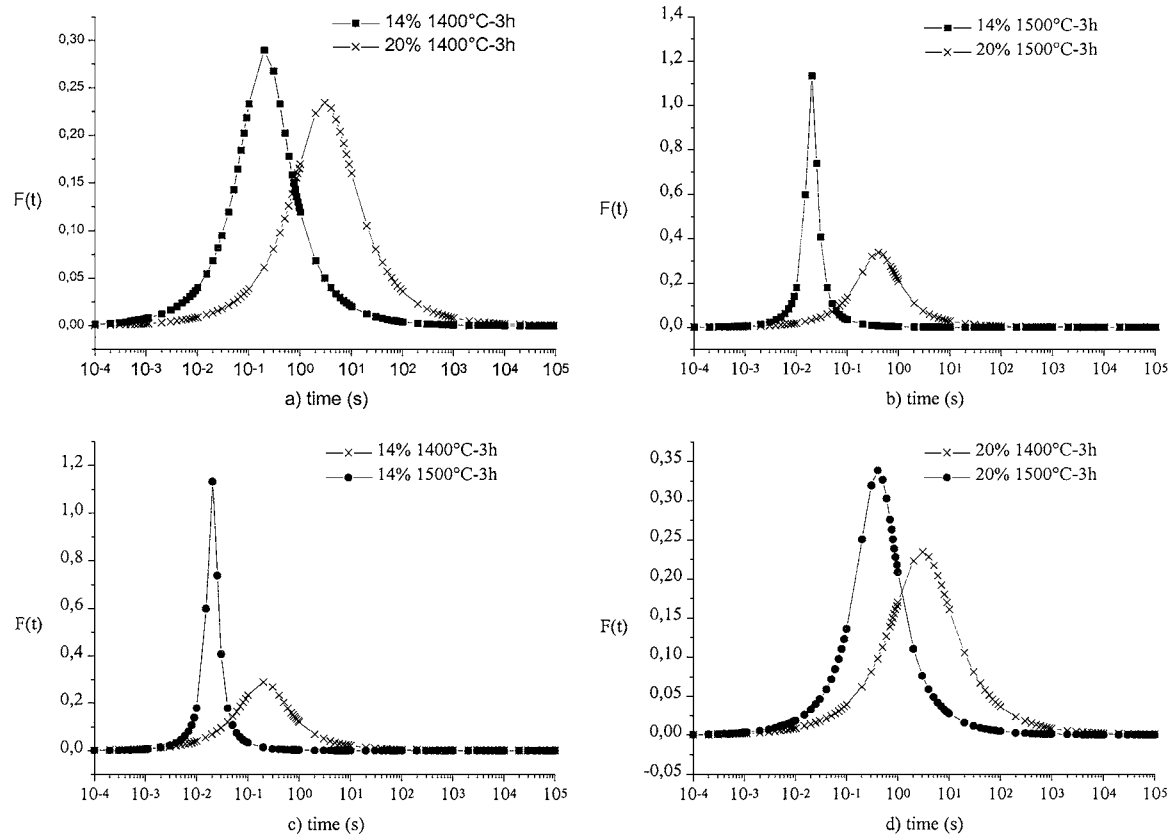

Figure 15 Distribution function of relaxation times. a) and b) effect of the tungsten volume fraction, c) and d) effect of the sintered temperature.

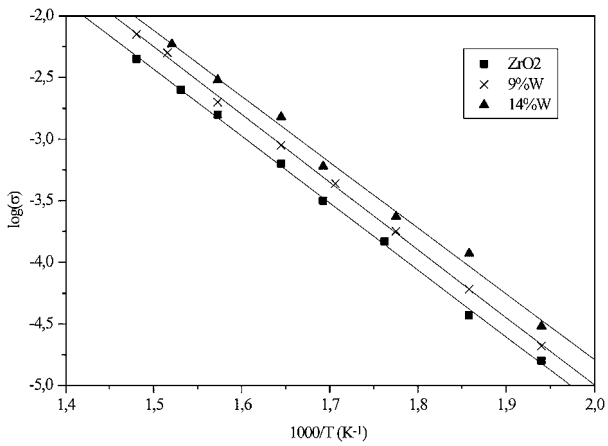

Figure 16 Arrhenius plots of the intragrain ionic conductivity for three compositions.

of the zirconia. Indeed, for a given temperature the ionic conductivity of zirconia increases with the metal volume fraction.

4. Conclusion

Stabilised zirconia-tungsten composites have been obtained starting from composite powders. Pressurless sintering leads to composites with an open porosity whatever is the metal volume fraction, hot pressing is then necessary to densified the material. The influence of the metal volume fraction on the samples morphology has been evidenced, indeed no zirconia agglomerates are present in the composite for metal volume fractions above 20%. During the sintering step the linear shrinkage greatly depends on the tungsten volume fraction. The microhardness of the sintered materials decreases with increasing the metal volume fraction as well as the thermal expansion coefficients which lie between the Turner and the Kerner model.

The electrical resistivity of the composites has been fitted using the general effective medium equation. According to this model, the percolation threshold is 0.26 and the *t* parameter is 3.5. The impedance spectroscopy allows to show that high temperature treatments lead to a better ceramic-metal interface and that space charges polarization is an important phenomenon in ceramic-metal composites. Ionic conductivity measurements indicate that the intragrain zirconia ionic condiuctivity is improved when the tungsten volume fraction increases.

References

1. W. H. TUAN and R. J. BROOKS, *J. Europ. Ceram. Soc.* **6** (1990) 31.
2. E. BREVAL, *J. Mater. Sci.* **27** (1992) 1464.
3. S. VIVES, C. GUIZARD, L. COT and C. OBERLIN, *ibid.* **34** (1999) 3127.
4. F. ZOK and F. F. LANGE, *J. Amer. Ceram. Soc.* **74**(8) (1991) 1880.
5. J. L. SHI, J. H. GAO, Z. X. LIN and D. S. YAN, *J. Mater. Sci.* **28** (1993) 342.
6. M. S. KALISZEWSKI and A. H. HEUER, *J. Amer. Ceram. Soc.* **73**(6) (1990) 1504.
7. R. P. INGEL and D. LEWIS, *ibid.* **69**(4) (1986) 325.
8. P. PASCAL, "Nouveau Traite De Chimie Minerale," tome XIV Ed (Masson, Paris, 1959).
9. R. A. CULTER, J. R. REYNOLDS and A. JONES, *J. Amer. Ceram. Soc.* **75**(8) (1992) 2173.
10. C. H. FAN and M. N. RAHAMAN, *ibid.* **75**(8) (1992) 2056.
11. M. N. RAHAMAN and L. C DE JONGHE, *ibid.* **74**(2) (1991) 433.
12. G. W SCHERER, *ibid.* **70**(10) (1987) 719.
13. R. K. BORDIA and G. W SCHERER, *Acta. Met.* **36**(9) (1988) 2411.

14. R. P INGEL, D. LEWIS, B. A. BENDER and R. W. RICE, *Adv. Ceram.* **12** (1984) 408.
15. Metals Handbook Vol 1, *Properties and Selection of Metals*, 8th ed. (Taylor-Lyman, Metals Park, Ohio, 1967).
16. P. S. TURNER, *J. Res. Natl.Bur. Std.* **37** (1952) 243.
17. E. H. KERNER, *Proc. Phys. Soc.* **69B** (1956) 808.
18. D. S. MCLACHLAN, M. BASZKIEWICZ and R. E. NEWNHAM, *J. Amer. Ceram. Soc.* **73**(8) (1990) 2187.
19. "Handbook of Chemistry and Physics," 58th ed. (1977–1978) edited by R. C. Weast.
20. J. DE DIOS SOLER, M. A. PEREZ-JUBINDO, A. DOMINGUEZ-RODRIGUEZ and A. H. HEUER, *J. Amer. Ceram. Soc.* **72**(8) (1989) 1500.
21. IN-GANN CHEN and W. B. JOHNSON, *J. Mater. Sci.* **26** (1991) 1565.
22. B. ABELES, H. L. PINCH and J. I. GITTLEMAN, *Phys. Rev. Lett.* **35** (1975) 247.
23. J. KOVACIK, *Script. Mater.* **39**(2) (1998) 153.
24. J. WU and D. S. MCLACHLAN, *Physica A.* **241** (1997) 360.
25. C. CHITEME and D. S. MCLACHLAN, *Physica B.* **279** (2000) 69.
26. K. H. COLE and R. H. COLE, *J. Chem. Phys.* **9** (1941) 341.
27. L. F. SCHELP, E. L. ROSA, J. L. MAURICE, F. PETROFF and A. VAURES, *J. Magn. Magn. Mater.* **205** (1999) 170.
28. J. LU, L. GAO, J. SUN, L. GUI and J. GUO, *Mater. Sci. Eng.* **A293** (2000) 223.
29. E. J. L. SCHOULER, N. MESBAHI and G. VITTER, *Sol. Stat. Ion.* **9/10** (1983) 989.

Received 6 March 2000
and accepted 21 May 2001